

A combined neuronal and mechanical model of fish swimming

Örjan Ekeberg

Department of Numerical Analysis and Computing Science, Royal Institute of Technology, S-100 44 Stockholm, Sweden
Nobel Institute for Neurophysiology, Karolinska Institute, S-104 01 Stockholm, Sweden

Received: 6 November 1992/Accepted in revised form: 21 April 1993

Abstract. A simulated neural network has been connected to a simulated mechanical environment. The network is based on a model of the spinal central pattern generator producing rhythmic swimming movements in the lamprey and the model is similar to that used in earlier simulations of fictive swimming. Here, the network has been extended with a model of how motoneuron activity is transformed via the muscles to mechanical forces. Further, these forces are used in a two-dimensional mechanical model including interaction with the surrounding water, giving the movements of the different parts of the body. Finally, these movements are fed back through stretch receptors interacting with the central pattern generator. The combined model provides a platform for various simulation experiments relating the currently known neural properties and connectivity to the behavior of the animal *in vivo*. By varying a small set of parameters, corresponding to brainstem input to the spinal network, a variety of basic locomotor behaviors, like swimming at different speeds and turning can be produced. This paper describes the combined model and its basic properties.

1 Introduction

In order to understand the function of a neural network, it is generally not sufficient to know the properties of the neurons and the connectivity in detail. The character of the input and the output also plays a crucial role. Biologically characterized networks might not operate naturally without the proper environmental input. Further, this input is often dependent on network output, thus requiring a model of the environment in which the network operates. Formulating such an environment model, capable of providing a realistic feedback, becomes essential when doing computer simulations of this kind of networks. When the network under study is connected more or less directly to muscular output and sensory

input, some representation of the mechanical environment is needed. This requires modeling muscles and receptors, including their interaction with the neurons, as well as the mechanical environment, including relevant parts of the body (cf. Grillner 1981).

In some experimental preparations, most of the neural communication with other subsystems can be disconnected, making it possible to study the behavior of the neural network in isolation. One such preparation is the isolated spinal cord of the lamprey, in which the central pattern generator producing rhythmic locomotor activity (swimming) can be activated despite the lack of both brainstem input and sensory feedback (Grillner et al. 1981b; Brodin et al. 1985). During such fictive swimming, many characteristic features of real swimming may be preserved, e.g., the possibility to "swim" at different speeds and the phase shift of motoneuron output between different points along the cord (Wallén and Williams 1984).

One approach to realistic simulation of biologically characterized networks is to restrict the simulations to such isolated systems. Indeed, computer simulations of the lamprey central pattern generator have been successful in explaining most observations during fictive swimming (Wallén et al. 1992; Wadden et al. 1993) in terms of realistically simulated neurons (Ekeberg et al. 1991; Brodin et al. 1991) and a synaptic connectivity based on known connections from paired intracellular recordings (Grillner et al. 1991). However, restricting the use of realistic simulations only to model such isolated preparations is not desirable. For example, in order to relate the simulated neuronal activity to normal swimming and also to study the role of the sensory feedback it is necessary to include some representation of the mechanical environment.

Many general aspects of swimming behavior of fish have been studied (J. Gray 1933b; Lighthill 1969; Grillner and Kashin 1976; Webb and Weihs 1983). There are also similar studies directed more specifically towards the lamprey in particular (Wallén and Williams 1984; Williams et al. 1989). The lamprey has a slender body without paired fins. It swims by propagating an undulatory wave with increasing amplitude from head to tail. These undulations are caused by rhythmic motoneuronal activity alternating between the two sides of the spinal

Correspondence to: Ö. Ekeberg, Department of Numerical Analysis and Computing Science, Royal Institute of Technology, S-100 44 Stockholm, Sweden

cord (Grillner 1974). The alternations occur later at more caudal positions along the body, with a lag proportional to the distance between the points. Thus, a wave of motoneuronal activity is produced which propagates caudally during normal swimming. The phase lag between any pair of points along the cord stays constant even when the speed of swimming changes.

The aim of the current work has been to construct a model of the neural control of swimming that is suitable for computer simulation. This includes both the mechanical movements and the neural control system. Mechanical models in connection with neural models have earlier been used to study, for example, the neural control of bipedal walking (Taga et al. 1991) and arm movements (Kalveram 1991). In those studies, however, the neural component was based on abstract oscillators or pattern generators rather than experimentally characterized neural networks. A mechanical model of how enforced muscle forces give rise to body movements in the swimming lamprey has also been formulated (Bottell and Williams 1991). That study, however, did not include any forces from the surrounding water.

Here, the neural network model of the spinal central pattern generator is similar to that used in the simulations of fictive swimming in the lamprey. However, the model neurons are simpler and the network is also connected to a simulated mechanical environment. The neural network model has been extended with a mechanism by which motoneuron activity can be transformed via the muscles to mechanical forces. These forces are used in a two-dimensional mechanical model of the body, taking the interaction with the surrounding water into account when computing the movements of the different parts of the body. Finally, these movements are fed back through stretch receptors interacting with the central pattern generator.

2 The neural network model

The system simulated consists of two main parts: the neural network and the mechanical system. The neural network model is based on earlier simulations using detailed cell models and an experimentally established connectivity (cf. Wallén et al. 1992). In the present work, the individual model neurons have been simplified considerably while the connectivity is maintained.

In the detailed simulations, a five-compartment model was used for each neuron. Voltage-dependent sodium, potassium and calcium ion conductances were calculated using equations of the Hodgkin-Huxley type. Intracellular calcium pools and calcium dependent potassium channels were also included. These model neurons are capable of producing realistic action potentials at various frequencies and also show effects like spike frequency adaptation (Ekeberg et al. 1990, 1991). Synaptic connections were modeled as transmembrane conductances and also included the voltage-sensitive *N*-methyl-D-aspartate (NMDA) receptors (Brodin et al. 1991).

Here, a simplified model neuron was constructed to enable simulation of the rhythm-generating network of

the entire spinal cord. A non-spiking model was chosen, in which each unit could be regarded as a representative of a population of functionally similar neurons. The output of each unit represents the mean firing frequency of the population. Measurements were made on the simulated neurons used in our earlier work (Ekeberg et al. 1991; Wallén et al. 1992) and the results were used when designing the simplified model. Important properties like input-output relations and spike frequency adaptation were basically preserved. The special NMDA properties, known to be important during slow swimming (Brodin et al. 1985), were not included in order to keep the model simple.

Simplified model neurons have earlier been used to study this neural system (Buchanan 1992). In that work, the model neurons displayed a qualitative behavior like real neurons, but no attempt was made to tune the model neuron parameters quantitatively. The model neurons used here are of similar complexity, but in addition they have been tuned to match the detailed neuron model used earlier.

The model neuron used here acts primarily as a "leaky integrator" with a saturating transfer function (Fig. 1A). The excitatory and the inhibitory synaptic

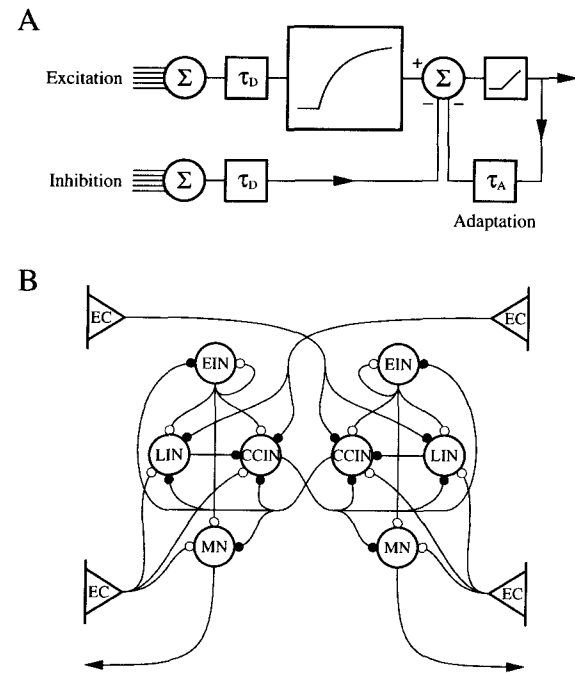


Fig. 1. A Basic mechanisms included in the neuron model. Excitatory and inhibitory synaptic inputs are added separately and subject to dendritic time delays. The excitatory input is transformed by the transfer function, while the inhibition is subtracted from the result. Adaptation is included as a delayed negative feedback. B Known connections between neurons of different types at the segmental level. The function of the network is briefly as follows: Excitatory interneurons (EIN) maintain activity ipsilaterally by exciting all the other cells; contralateral inhibitory interneurons (CCIN) suppress contralateral activity; lateral inhibitory interneurons (LIN) finally come in and terminate the ipsilateral activity. Motoneurons (MN) provide the output to the muscles, and edge cells (EC) are stretch-activated cells that excite the ipsilateral side and inhibit the contralateral side

inputs are added separately and are both subject to a dendritic time delay with a time constant τ_D . The excitatory input is then transformed by a function which provides saturation at high levels of excitatory input. The inhibitory input is subtracted from the result. Spike frequency adaptation is also included as a delayed negative feedback with another time constant, τ_A . Negative final values give an output of zero.

The delayed values for the excitatory synaptic input (ξ_+), the inhibitory synaptic input (ξ_-), and the neuron output (ϑ) are calculated from first-order differential equations:

$$\begin{aligned}\dot{\xi}_+ &= \frac{1}{\tau_D} \left(\sum_{i \in \Psi_+} u_i w_i - \xi_+ \right) \\ \dot{\xi}_- &= \frac{1}{\tau_D} \left(\sum_{i \in \Psi_-} u_i w_i - \xi_- \right) \\ \dot{\vartheta} &= \frac{1}{\tau_A} (u - \vartheta)\end{aligned}\quad (1)$$

Here, Ψ_+ and Ψ_- are the sets of incoming excitatory and inhibitory synapses respectively, w_i is the strength of synapse i , and u_i is the output value from the corresponding presynaptic neuron. Now, the output from the model neuron is given by:

$$u = \begin{cases} 1 - \exp\{(\Theta - \xi_+) \Gamma\} - \xi_- - \mu \vartheta & \text{if positive} \\ 0 & \text{otherwise} \end{cases} \quad (2)$$

Here, Θ is a threshold for activation, Γ is a gain constant, and μ controls the level of adaptation. The maximum output has here been normalized to one by scaling the synaptic weights appropriately.

The simulated neural network contains neurons of five different types: motoneurons (MN), excitatory interneurons (EIN), lateral inhibitory interneurons (LIN), contralateral inhibitory interneurons (CCIN), and stretch-sensitive edge cells (EC). Except for the sensory edge cells, populations of neurons are modeled as described. The parameters for each model neuron were tuned to match the response characteristics of the corresponding neuron type from the detailed simulations (Ekeberg et al. 1991; Wallén et al. 1992). The resulting values are shown in Table 1.

In the earlier simulations, the neurons modeled in a realistic fashion were interconnected into a network in accordance with experimentally established synapses (Fig. 1B). The synaptic parameters were then tuned to produce a behavior consistent with that observed during fictive swimming (Wallén et al. 1992). Here, the corresponding synapse parameters were used to connect the simplified neurons in each segment.

The segmental network as shown in Fig. 1B is repeated along the spinal cord. Here, 100 such segments are included, giving a total of 1000 neurons (only one EC on each side needs to be simulated, representing both excitatory and inhibitory EC). In addition to the segmental connectivity, the neurons are also connected to neighboring segments along the spinal cord, but the connectivity between segments is not known in detail. Different

mechanisms have been suggested to explain the constant phase lag seen between different points along the cord: locally increased excitability (Matsushima and Grillner 1992) or asymmetrical coupling between segmental oscillators (Williams 1992). The differences between the suggested mechanisms were not addressed here. Rather, an intermediate position was taken by utilizing both asymmetrical coupling and locally increased excitability.

The synaptic output from each neuron is distributed to receiving neurons in nearby segments both caudally and rostrally, using the same synaptic strength as within the segment. The extent of this distribution is set individually for each type of connection, roughly based on the known extent of the corresponding projections in the lamprey. The extents used, in terms of number of segments, are given in Table 2 together with the other synaptic parameters.

This network is capable of producing a rhythmic pattern of activity at various frequencies when tonic brainstem input is provided. Further, coordinated waves of activity along the spinal cord are generated, in particular when the tonic input to the five most rostral segments is increased. This is in accordance with experimental

Table 1. Neuron parameters

Neuron type	Θ	Γ	τ_D	μ	τ_A
EIN	-0.2	1.8	30 ms	0.3	400 ms
CCIN	0.5	1	20 ms	0.3	200 ms
LIN	8	0.5	50 ms	0	—
MN	0.1	0.3	20 ms	0	—

EIN, Excitatory interneuron; CCIN, contralateral inhibitory interneuron; LIN, lateral inhibitory interneuron; MN, motoneuron

For each neuron type, the parameters used in (1) and (2) are given: Θ , firing threshold; Γ , gain; τ_D , dendritic time constant; μ , adaptation; τ_A , time constant of adaptation

Table 2. Synapse parameters

Pre synaptic neuron	Post synaptic neuron	Type	Strength	Rostral extent	Caudal extent
EIN	EIN	Ex	0.4	2	2
EIN	CCIN	Ex	3	2	2
EIN	LIN	Ex	13	5	5
EIN	MN	Ex	1	5	5
CCIN	EIN	Inh	2	1	10
CCIN	CCIN	Inh	2	1	10
CCIN	LIN	Inh	1	1	10
CCIN	MN	Inh	2	5	5
LIN	CCIN	Inh	1	5	5
EC	CCIN	Inh	0.01	0	0
Brainstem	EIN	Ex	2	—	—
Brainstem	CCIN	Ex	7	—	—
Brainstem	LIN	Ex	5	—	—
Brainstem	MN	Ex	5	—	—

The model neurons are connected according to Fig. 1B but also to the same neurons in neighboring segments. The "extent" denotes how far these connections reach (in number of segments) in the rostral and caudal direction. The connection weight (w_i) used in (1) is the "strength" given here divided by the number of segments it connects to. Ex, Excitatory; Inh, inhibitory

findings for the isolated spinal cord of the lamprey (Matsushima and Grillner 1992) as well as with simulation results using the detailed neuron model (Wadden et al. 1993).

3 The mechanical model

The second main component of the system simulated is the mechanical model. The actual swimming movements are calculated using a two dimensional mechanical model of the body considering also the forces from the surrounding water. The neural network model interacts with the mechanical model in two ways: (1) the output of the model motoneurons controls the spring constants of the model muscles; (2) information about the curvature of the body is fed back to the neural network via the stretch-sensitive EC.

In order to mathematically describe the position and shape of the body as it varies in time, the projection of the midline on the horizontal plane is used. The position of this curve is represented by a chain of N links connected by $N - 1$ joints (Fig. 2B). In the simulations presented here, N was set to 10, implying that each mechanical link corresponds to 10 neural segments. An alternative view would be to keep a curve representation of the body. Such a formulation would lead to partial differential equations describing the forces and the motion. Here, however, the formulation as a chain of links was chosen because of the direct correspondence with the numerical solution.

The links are numbered from the head to the tail, and the position of each link i is described by three coordinates x_i , y_i , and φ_i : x_i and y_i denote the position of the midpoint of the link, while φ_i denotes the angle from the x -axis (see Fig. 2A). This set of parameters constitutes

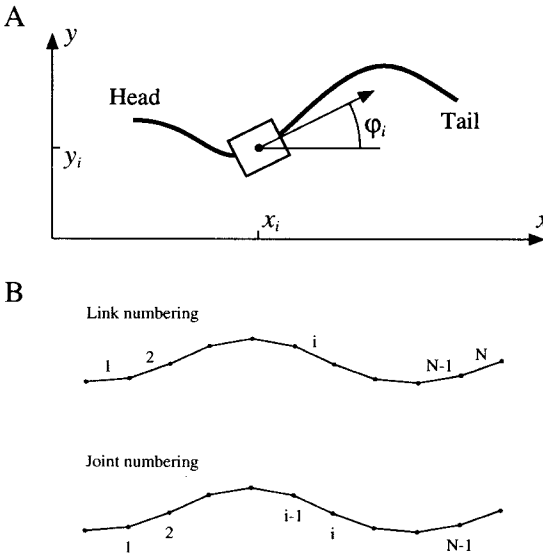


Fig. 2A, B. Representation of the fish body as a chain of interconnected links. **A** The position of each link i is described by the position of its midpoint (x_i, y_i) , which is also its center of gravity, and its direction φ_i . **B** The links and joints are numbered from the head towards the tail

a non-minimal representation of the position of the body, implying that the mechanical constraints have to be explicitly stated in order to solve the kinematic equations. The movement of the links is here constrained by the joints, forcing them to stay connected. This constraint can be expressed mathematically as:

$$\begin{aligned} x_i + \frac{l_i}{2} \cos \varphi_i &= x_{i+1} - \frac{l_{i+1}}{2} \cos \varphi_{i+1} \\ y_i + \frac{l_i}{2} \sin \varphi_i &= y_{i+1} - \frac{l_{i+1}}{2} \sin \varphi_{i+1} \end{aligned} \quad \text{where } i \in \{1, \dots, N-1\} \quad (3)$$

Here, l_i is the length of link i .

Each link i is acted upon by three types of forces (Fig. 3A): muscular torques T_i and T_{i-1} , water forces \bar{W}_i , and inner forces from neighboring links \bar{F}_i and \bar{F}_{i-1} . Once these different forces are known, the movement can be calculated by integrating the accelerations from Newton's law of motion:

$$\begin{aligned} m_i \ddot{x}_i &= W_{i,x} + F_{i,x} - F_{i-1,x} \\ m_i \ddot{y}_i &= W_{i,y} + F_{i,y} - F_{i-1,y} \\ I_i \ddot{\varphi}_i &= T_i - T_{i-1} - (F_{i-1,x} + F_{i,x}) \frac{l_i}{2} \sin \varphi_i \\ &\quad + (F_{i-1,y} + F_{i,y}) \frac{l_i}{2} \cos \varphi_i \end{aligned} \quad \text{where } i \in \{1, \dots, N\} \quad (4)$$

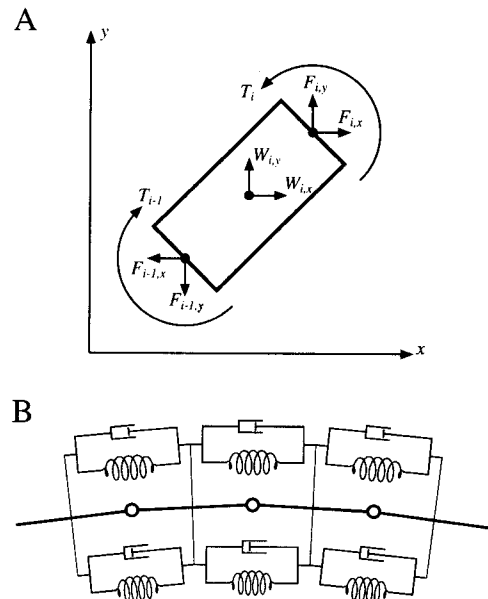


Fig. 3. **A** Forces acting on link i : muscular torques T_i and T_{i-1} , water forces \bar{W}_i , and inner forces from neighboring links \bar{F}_i and \bar{F}_{i-1} . **B** The bending torques on the body are controlled by the activation of muscles on both sides of the body. The spring constants for the muscles are changed by the activity in the corresponding MN. This model gives the possibility for the neural network to vary both the total bending force and the stiffness locally along the length of the body

Here, m_i is the mass and I_i the moment of inertia. The torques and inner forces at the end-points ($i = 0$ and $i = N$) are all zero.

3.1 Body parameters

In order to use (4), values for the masses and the moments of inertia for all the links are needed. These are estimated from the shape and density of the corresponding part of the body. Since the neural network model was derived from experiments on the lamprey, the body was also chosen to correspond roughly to the lamprey in size and shape. The method is general enough to be applicable to many other species. We will use the term "fish" below to denote our model animal, though the lamprey strictly speaking is a cyclostome.

The body shape chosen is 30 cm long and has no pronounced fins. The cross sections are elliptical with a height of 3 cm. In a typical fish, the height would decrease caudally, but fins and the flattened shape could compensate somewhat for this effect (cf. below). Here, the same height has been used along the entire body. In the rostral part, the width is 2 cm but after about one third of its length, the width decreases linearly towards the tail.

Since the mean density of a fish is the same as that of water, it is reasonable to estimate the mass of each link from the volume of a corresponding piece of the body. This gives the values found in Table 3. The moment of inertia for a link is estimated from that of an elliptical cylinder:

$$I = m \left(\frac{w^2}{16} + \frac{l^2}{12} \right)$$

where m is the mass, w the width, and l the length of the cylinder (see, e.g., D. E. Gray 1972). Inserting values corresponding to the shape of the body gives the values found in Table 3.

3.2 Water forces

The hydrodynamic aspects of swimming have been described in various models (Wu 1971; Blake 1983; Yates 1983). Forces acting on the body from the surrounding

Table 3. Mechanical properties of the links

Link	l_i (cm)	m_i (g)	I_i (g mm)	λ_\perp (Ns ² /m ²)	λ_\parallel (Ns ² /m ²)
1	3	4.5	45.0	0.045	0.030
2	3	4.5	45.0	0.045	0.020
3	3	4.5	45.0	0.045	0.010
4	3	4.5	45.0	0.045	0
5	3	3.8	35.6	0.045	0
6	3	3.15	27.5	0.045	0
7	3	2.5	20.4	0.045	0
8	3	1.8	14.2	0.045	0
9	3	1.1	8.6	0.045	0
10	3	0.45	3.4	0.045	0

For each link, the length (l_i), mass (m_i), and moment of inertia (I_i) are given along with the estimated water resistance coefficients λ_\perp and λ_\parallel for the flow perpendicular and parallel to the body, respectively

water depend on the speed of the body relative to the water. At very low speeds the viscous forces are important, while at higher speeds inertial effects play the dominating role. Here, we assume that the inertial forces dominate (high Reynolds numbers). In principle, it would be possible to simulate the complete three-dimensional flow around the fish body, which would give the forces on the body. This kind of simulation, however, is very time consuming. Reasonable approximations for the forces can be obtained by viewing the surrounding water as stationary and considering the forces on each link from its speed alone (cf. Taylor 1952).

Movement of any object through a stationary fluid causes an increase in pressure in front of the object and a decrease behind it. This makes the fluid in front move away and return again behind the object. The different pressures on the two sides also give a net drag force on the object, counteracting the movement. This force is proportional to the square of the speed and can be calculated from:

$$W = \rho v^2 \frac{A}{2} C \quad (5)$$

where ρ is the density of the fluid, v is the speed of the object, A is the area perpendicular to the movement, and C is the drag coefficient given by the shape of the object (see, e.g., Blevins 1984). For water we have $\rho = 1000 \text{ kg/m}^3$. Here, λ will be used as an abbreviation for $\rho A C / 2$. For simplicity, we will assume that the pressure differences resulting from movements along the body are added linearly to those from movements perpendicular to the body. Thus, movements in these two directions are handled separately and the resulting forces are added to give the combined effect. The sizes of the parallel force component (W_\parallel), and the perpendicular force component (W_\perp) are rewritten as:

$$W_\parallel = v_\parallel^2 \lambda_\parallel \quad W_\perp = v_\perp^2 \lambda_\perp \quad (6)$$

where v_\parallel is the parallel component and v_\perp the perpendicular component of the velocity v and λ_\parallel and λ_\perp are the corresponding λ factors, estimated from (5).

Movements perpendicular to the body axis are the most important ones for propulsion. Since the cross sections are elliptical, it is reasonable to use data for drag forces on an elliptical cylinder in a moving fluid. When the ellipse is not too eccentric, the drag coefficient, C , is close to 1. Near the tail the flattened shape should really call for a higher C value. On the other hand, the height of a real fish usually decreases, compensating for this effect. Because of the approximate nature of these values, the value $C = 1$ has been used along the entire body. Note that since this fish-like body lacks a large tail fin, the movements are expected to be of the *anguilliform* (eel-like) type (see, e.g., J. Gray 1933b, 1968; Blake 1983).

For movements parallel to the body axis, forces are harder to estimate properly since they depend on how the shape of the cross section varies along the body. Explorative simulations have shown that the size of these forces does not influence the resulting swimming very much. We have assumed that these forces are negligible except

for the first three links where the cross-sectional area changes most dramatically. The values used for λ_{\parallel} given in Table 3 are estimated values based on the area of the cross section.

3.3 Muscles

The motoneurons of the network drive the various muscles, which in turn produce forces that cause movements of the body. The relevant muscles are located on the two sides of the body with their axis of contraction being mainly parallel to the main axis of the body. In reality, these muscles are not directly connected to the skeleton, but we will still assume that the length of the muscle fibers varies linearly with the local curvature of the body.

As a rule, muscles are modeled by including both an elastic and a viscous component (e.g., Lacquaniti and Soechting 1986). The elastic component can be viewed as a spring where the spring constant is used to set the force produced in a steady-state condition. The viscous component of the force is proportional to the speed of the movement. For simplicity, elastic and viscous forces from non-muscular parts of the body like the skin are included in the muscle model.

The motoneuronal output can be assumed to linearly control the forces generated by the muscles (cf. Tax and Denier van der Gon 1991). This corresponds to a linear relationship between motoneuronal activity and the muscular spring constant.

The local curvature in the chain model corresponds to the difference in angle between two consecutive links (Fig. 3B). The linear relationships assumed make it possible to express the torque acting at a particular joint as a linear function of the motoneuron activity on the two sides (M_L and M_R):

$$T_i = \alpha(M_L - M_R) + \beta(M_L + M_R + \gamma)(\varphi_{i+1} - \varphi_i) + \delta(\dot{\varphi}_{i+1} - \dot{\varphi}_i) \quad (7)$$

(see Appendix A for details). Four parameters are introduced: α is the gain of the muscles, β is the stiffness gain, γ is the tonic stiffness, and δ is the damping coefficient. Here, the same set of parameter values has been used throughout the body: $\alpha = 3 \text{ N mm}$; $\beta = 0.3 \text{ N mm}$; $\gamma = 10$; $\delta = 30 \text{ N mm ms}$. For a more detailed analysis, values measured at different points along the body would be desirable.

It should be noted that this arrangement makes it possible for the neural network not only to control the static torque (by setting $M_L - M_R$), but also to control the stiffness of the body (by setting $M_L + M_R$).

3.4 Stretch receptors

Changes in body curvature are known to influence the activity of the locomotor central pattern generator. In the lamprey, the receptors have been identified as stretch-activated EC located at the lateral margin within the spinal cord (Grillner et al. 1981a; Viana Di Prisco et al. 1990). When the body is bent, EC on the stretched side

become active. Inhibitory EC will then inhibit activity on the contracted side, while excitatory EC promote activity on the stretched side (cf. Fig. 1B).

The activity level of an EC is roughly proportional to the curvature of the body at the site of the cell (Grillner et al. 1982). The proportionality constant by itself is irrelevant and has been set to one. The strength values for the synapses from the EC are not known. Different settings have been tested but further work is needed to analyze the functional importance of each of these connections. In the simulations presented here, the only synapse used is the inhibitory input to CCIN (see Table 2). The output of an EC on the right side of the body is computed as:

$$f = \begin{cases} (\varphi_i - \varphi_{i+1}) \frac{2}{l_i + l_{i+1}} & \text{when } \varphi_i > \varphi_{i+1} \\ 0 & \text{otherwise} \end{cases} \quad (8)$$

The output of an EC on the left side is computed in a corresponding way.

3.5 Inner forces

In Newton's law of motion (4), the forces from the water can be estimated from (6), while the muscular torques are given by (7). The only forces left unknown are the inner forces $F_{i,x}$ and $F_{i,y}$. These forces act to enforce the mechanical constraint that the links must stay connected during the motion as expressed by (3). Equations (3) and (4) constitute a differential-algebraic equation system of the type generally encountered for mechanical multibody problems formulated using a non-minimal set of coordinates.

The kinematic constraints (3) can be written in compact form (see Appendix B for details):

$$\bar{g}(\bar{p}) = \bar{0} \quad (9)$$

where $\bar{g}(\bar{p})$ is a $2(N - 1)$ column vector.

The motion (4) can also be expressed in compact form (see Appendix B):

$$\dot{\bar{p}} = \bar{v} \quad \mathcal{M}\dot{\bar{v}} = \bar{w} + \mathcal{G}(\bar{p})\bar{f} \quad (10)$$

where \bar{p} is a $3N$ column vector composed of the position coordinates of all the links; \bar{v} is the corresponding speeds; \bar{w} is the external forces (water forces and muscle torques); \mathcal{M} is the $3N \times 3N$ diagonal mass matrix; and \bar{f} is a $2(N - 1)$ column vector containing the unknown inner forces. The matrix $\mathcal{G}(\bar{p})$ is actually the transpose of the jacobian of $\bar{g}(\bar{p})$. This is a consequence of the fact that the inner forces are introduced by the constraints. During the computation of \bar{f} , the position \bar{p} is assumed to be constant. Therefore, the arguments to \bar{g} and \mathcal{G} are left out in the equations below.

Differentiating (9) twice with respect to time gives an equation which can be written as (see Appendix B):

$$\mathcal{G}^T \dot{\bar{v}} = \bar{\pi} \quad (11)$$

Inserting the expression for $\dot{\bar{v}}$ from (10) into (11) gives:

$$\mathcal{G}^T \mathcal{M}^{-1}(\bar{w} + \mathcal{G}\bar{f}) = \bar{\pi}$$

which can be restated as a system of linear equations in $\bar{\mathbf{f}}$:

$$(\mathcal{G}^T \mathcal{M}^{-1} \mathcal{G}) \bar{\mathbf{f}} = \bar{\mathbf{p}} - \mathcal{G}^T \mathcal{M}^{-1} \bar{\mathbf{w}} \quad (12)$$

Note that \mathcal{M} is a constant diagonal matrix so the calculation of \mathcal{M}^{-1} is trivial. Solving (12) will give the inner forces $\bar{\mathbf{f}}$ which were the only missing components to calculate the accelerations from (10).

3.6 Numerical methods

The differential equations used in the neural model (1) are straightforward to integrate by any suitable numerical method. For simplicity, the Euler method was used with a step length of 10 ms.

Solving the equations describing the mechanical system is a bit more complicated. First, the inner forces $\bar{\mathbf{f}}$ are solved from the linear equation system (12) using gaussian elimination and pairwise pivoting between x and y coordinate directions. Since the left-hand side matrix $(\mathcal{G}^T \mathcal{M}^{-1} \mathcal{G})$ is a band matrix of width 6, solution is fairly quick even for large N 's.

The movement of the body is now calculated by integrating (10). With the current parameter settings, this equation system turns out to be stiff. The stiffness arises especially from the damping characteristics of the model muscles but also from the spring stiffness and the counteracting forces from the water. Stiffness of this type prevents large integration steps to be taken using an ordinary (explicit) numerical method because of numerical instability. The examples shown here were run with a step length of 1 ms where the simulations were numerically stable using the Euler method. By using another numerical formulation where the stiffness introduced by the muscle torques were handled implicitly, the step length could be increased to about 5 ms. It is likely that an iterative implicit method would make it possible to take even longer steps.

Simulations running on a Decsystem 5000/200 workstation using a step length of 1 ms for the mechanical system and 10 ms for the neural system are able to run at about one fifth of real time (with graphical output disabled). The speed is limited primarily by the mechanical simulation but also for practical purposes by the graphical output.

Only the second derivatives of the kinematic constraints (3) were used when solving the equations. Mathematically, this is perfectly correct as long as the initial values conform to (3). However, the numerical solution can run into severe problems when the numerical errors make the state variables violate the original constraints. This effect has been thoroughly analyzed recently (Alishenas 1992; see also Ólafsson and Alishenas 1992). A technique called *stabilization through projection* was suggested to continuously adjust the system to conform to the constraints. The adjustment is done by projecting the position and/or speed values down to the subspace formed by the kinematic constraints. Alishenas found that stabilization of the speed variables was critical while the adjustment of positions was less important. Here, the speeds are adjusted using this projection tech-

nique, while the positions are adjusted by using simple repositioning.

Speed stabilization through projection according to Alishenas (1992) is done by solving $\bar{\mathbf{x}}$ from:

$$(\mathcal{G}^T \mathcal{M}^{-1} \mathcal{G}) \bar{\mathbf{x}} = \mathcal{G}^T \bar{\mathbf{v}}$$

where $\bar{\mathbf{v}}$ are the numerically obtained approximate values for the speeds $\bar{\mathbf{v}}$. Note that the left-hand side of the equation system is the same as in (12) which has already been computed. The new stabilized speed values are now obtained from:

$$\bar{\mathbf{v}} = \bar{\mathbf{v}} - \mathcal{M}^{-1}(\mathcal{G} \bar{\mathbf{x}})$$

This stabilization need not be applied after each time step. Here, stabilization was done after every tenth integration step.

4 Simulation of propulsion and turning

In order to test to what extent the model captures various properties of normal swimming behavior, a number of simulations were done. Here, only a limited number of basic simulation results are presented, representing the general capabilities of the model. A more detailed analysis of the simulation results will be presented in a separate paper.

4.1 Propulsion

When a tonic, symmetric, excitatory input is applied to the simulated neural network, alternating activity on the left and right side of the spinal cord will appear. A relatively low level of excitation is first chosen (0.15, arbitrary units). By further increasing the tonic level by 70% on the first five segments, coordinated waves of activity start traveling down the spinal cord (Fig. 4 A1–5). This is in accordance with the earlier simulations of fictive swimming where more detailed neuron models were used (Wallén et al. 1992; Wadden et al. 1993). The resulting length of these neural waves is slightly shorter than the length of the spinal cord. This relationship is directly related to the phase lag between the segments, and can be controlled by changing the amount of extra excitation given to the first segments.

The neural waves include activity of the MN which causes time-varying forces to be exerted by the model muscles. In the mechanical model, these coordinated waves of muscle forces are transformed to body undulations, making the fish swim forwards (Fig. 4 B1–5). At this level of excitation, the resulting speed through water is about 0.4 m/s.

A number of characteristic features of anguilliform swimming can be observed. Firstly, the amplitude of the undulations increases from head to tail, which is in agreement with natural anguilliform swimming (J. Gray 1933b). Note that this is not caused by any increasing level of output from the neural circuitry but is a pure consequence of the mechanical arrangement. Secondly, the mechanical wave of the body is faster than the speed

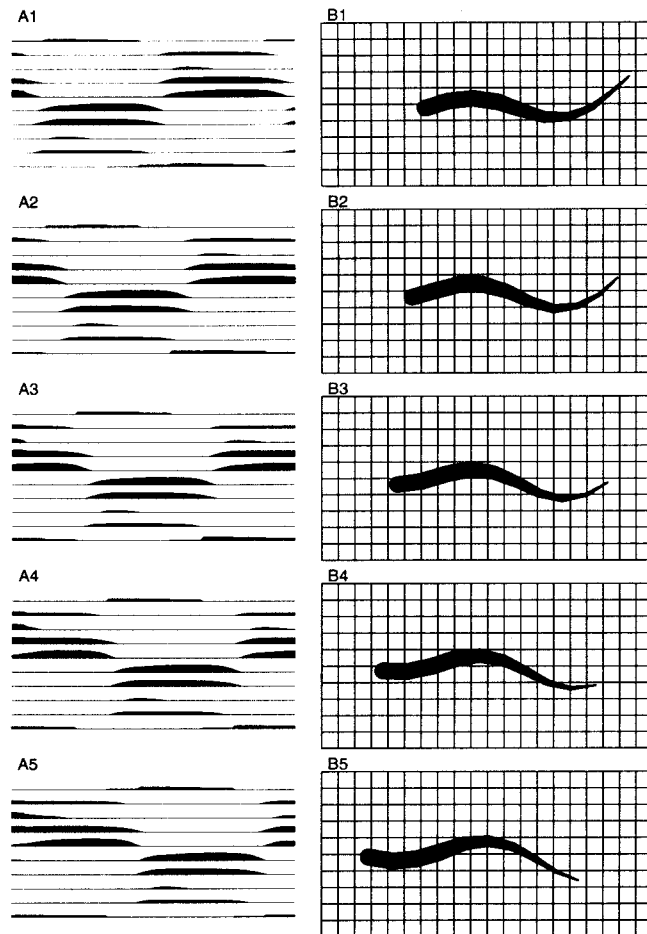


Fig. 4A, B. Steady-state swimming induced by low tonic excitation to the neural network. **A1–5** The neuronal activity; **B1–5** the corresponding position of the body. The interval between successive frames is 50 ms. In each frame **A1–5**, the neuronal activity is drawn in the following order from the top: right EC, MN, LIN, EIN, CCIN, left CCIN, EIN, LIN, MN, EC. Rostral is left and caudal is right. Grid lines below the body in **B1–5** are separated by 2 cm. Here, the stimulation level is 0.15 (arbitrary units) resulting in oscillations at 2.3 Hz and a speed through water of 0.4 m/s

through water. This can be observed by noting that the points of maximum body curvature move backwards in relation to the grid lines (Fig. 4 B1–5), and is a well-known property of most undulatory modes of swimming (Lighthill 1969).

Increasing the level of excitation increases the frequency of the oscillations. If the extra excitation to the first five segments is kept at 70%, the phase relations along the body will stay approximately the same when the excitation level is changed. Figure 5 shows the result when the level is set at 0.4 (arbitrary units). The higher frequency in combination with the constant phase relations makes the waves of neural activity move faster along the spinal cord. Consequently, the speed of swimming increases. Here it reaches a value of 0.73 m/s. The higher level of excitation also increases the amplitude of the neural activity, especially in the MN. This gives the increased muscular force needed to maintain the higher

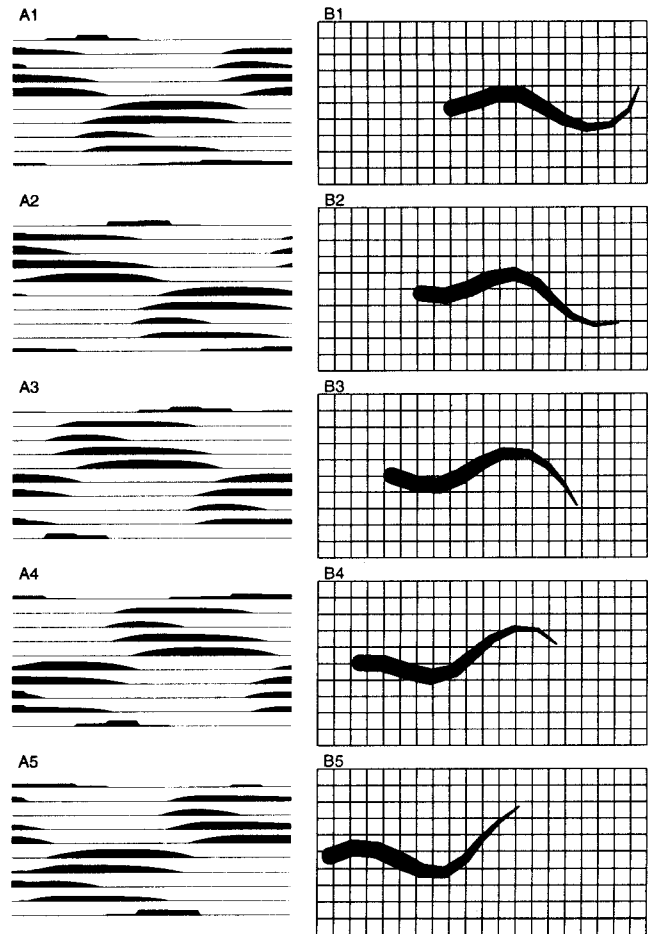


Fig. 5A, B. Steady-state swimming with a higher level of tonic excitation. Stimulation level is 0.4 (arbitrary units) resulting in oscillations at 4 Hz and a speed of 0.73 m/s

speed, and, as a consequence, the undulations become more pronounced.

The input from the stretch receptors (top and bottom traces in Fig. 5 A1–5) is out of phase with the motoneuronal activity by about 90°. The stretch receptors are maximally active at the time when the network is switching from contralateral to ipsilateral activity. This makes their input suited for terminating the contralateral activity at a time coordinated with the actual movement of the body. Thus, stretch receptor input may act as yet another burst-terminating factor in addition to those intrinsic to the neural network (cf. Wallén et al. 1992).

4.2 Turning

By making the tonic stimulation asymmetric it is possible to induce a turn (Fig. 6). An asymmetric component has here been added on top of the tonic level used in Fig. 5 by increasing the level by 0.3 on the right-hand side of the spinal cord and decreasing it by the same amount on the other. The neural network continues to produce waves of activity alternating between the two sides (Fig. 6 A1–5). The frequency and length of the bursts is about the same

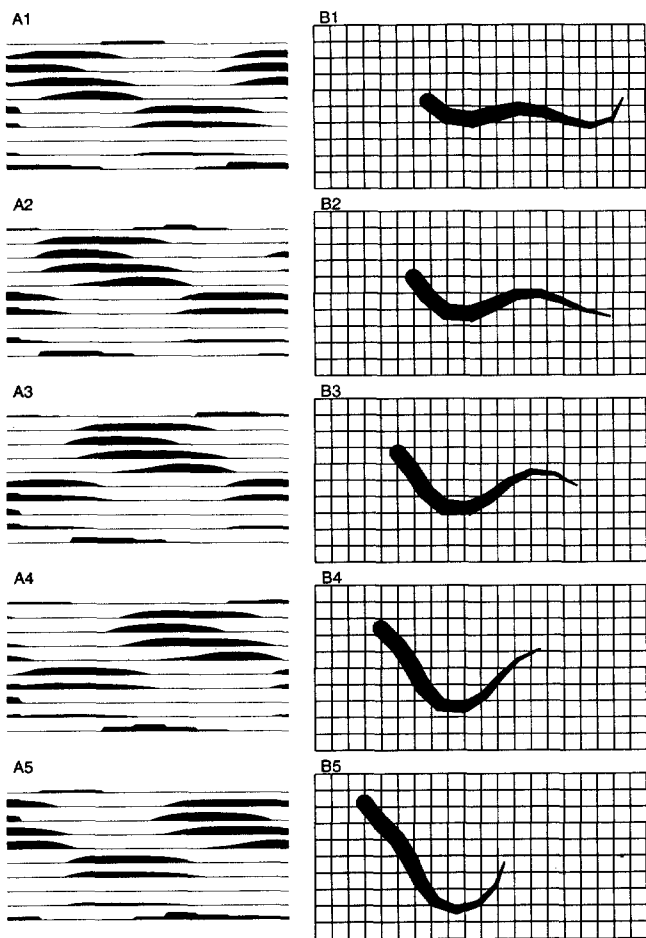


Fig. 6A, B. Steady-state swimming with asymmetric tonic excitation. The left side is stimulated with a level of 0.1 and the right with 0.7, producing a turn to the right

as before. The main difference is that the amplitude of the neural activity has become asymmetrical. The MN output on the right side is much larger than on the left. Note also that most LIN on the left side are silent.

In the mechanical system (Fig. 6 B1–5) the asymmetry in MN output amplitude gives the body a point of extra high curvature that propagates backwards along the body. This is consistent with observations on how real fish make turns (J. Gray 1933a). In Fig. 6, the asymmetrical stimulation was added immediately before the recording was made. If this asymmetrical stimulation is maintained, the fish will continue to swim in a circle.

5 Discussion

The combined neural and mechanical model presented in this paper has been constructed out of simplified components. Still, the behavior of the model is in many respects comparable with the basic swimming patterns seen for real animals.

The neural network model is based on an earlier more realistic model but uses much simpler neuronal elements. In particular, the individual spikes of the neurons are not represented. Further, the NMDA pacemaker properties are not included, which makes it impossible to produce very slow rhythms. However, the network used is capable of producing rhythmicity at different frequencies, and the intersegmental coupling makes it possible to generate natural waves of activity controllable by a small number of input parameters.

The mechanical model includes simplifications both with regard to the biological relevance of the parameters and equations used to describe the body and with regard to the forces from the surrounding water. For example, muscle activity produces a torque not only locally but, rather, over some distance along the body. However, the simplifications serve to remove less relevant details, making the model easier to understand and analyze. Whenever the model is found not to behave like the biological counterparts in important aspects, these simplifications have to be reconsidered. If additions to the model are found necessary, these will not only make the model more realistic. More importantly, findings of this kind may also add to the knowledge of the swimming process as such.

The swimming produced by the model presented here is of the anguilliform type. In order to apply the model to other types of swimming, some modifications have to be carried out. At present, the strength and stiffness of the muscles are constant throughout the body. This might be a reasonable approximation for an eel-like fish, but for other species the amount of muscles available at different points varies considerably.

Further, during anguilliform swimming, the entire body is moved back and forth in the transverse direction in order to produce the counteracting forces from the water needed for propulsion. For many other types of swimming, the effects of the paired pectoral fins and the unpaired dorsal and tail fins are much more important (cf. J. Gray 1968). Fins acting mainly by increasing the cross-sectional area exposed to the water are easily included in the current model by using a larger value for λ_1 at the site of the fin. However, when the fins produce substantial wakes, the view of the water as locally stationary is no longer valid and a more sophisticated water model might be needed. In general, when a certain species of fish is to be simulated, measured values for both water forces and muscle parameters would be desirable.

The role of the stretch sensitive edge cells has not been investigated extensively in this study. The strengths and relative importance of the different connections from these cells are not known in detail. In the simulations presented here, a relatively weak inhibitory connection to the CCIN is included which helps terminate the activity in synchrony with the mechanical undulations. To investigate the role of the EC and their different connections, further simulation studies are needed. A combined neural and mechanical model, such as the one presented here, should be a suitable platform for this task.

It is interesting to note that the neural network has the ability to control not only the forces bending the

body but also the tonic stiffness level. From (7), one can see that the bending forces are set by the difference in motoneuronal output from the two sides, while the stiffness is controlled by their sum. During fast swimming, the activity level of the MN is high, which also makes the body stiffer. This stiffness increases the intrinsic mechanical frequency of the body to better match the higher output frequency of the neural pattern generator. To further investigate the significance of such a resonance between the neural and the mechanical oscillations during swimming, muscle and body parameters based on quantitative measurements on a real fish should be used.

6 Conclusions

Computer simulation techniques make it possible to synthesize pieces of detailed knowledge from various sources and explore the consequences. Here, experimental data from neurophysiology, biophysical properties of muscles, and hydromechanical properties of water have been combined to study the behavior of swimming. By selecting or constructing models at an appropriate level of simplification for each component and using simulation techniques developed for constrained multibody dynamics, a model of fish swimming has been constructed and simulated. The combined neuro-mechanical model has proven capable of producing realistic swimming movements. By varying only the tonic level of excitation, corresponding to brainstem input to the neural network, swimming at different speeds and also turning can be produced. The behavior during other types of stimulation can be analyzed using the same model.

All the components have been simplified from more detailed knowledge. This model should therefore serve as a suitable platform for testing more detailed models of any of the components. In particular, the effects of various properties of the edge cells could be tested. Similarly, the consequences of fins and other changes to the body shape could be investigated by modifications and additions to these parts of this model.

Models of such a complex system as the neural control of vertebrate locomotion can be formulated at various levels of abstraction. While models including all known details are appealing for their completeness, their complexity and the lack of correspondingly exact parameter values limit their usefulness. On the other hand, models at a purely behavioral level can be hard to relate to known facts about the neurons and their connectivity. Here, an intermediate position has been taken by gradually simplifying a detailed model of the neuronal system while extending it with a mechanical environment. Because the components of the model can all be traced back to their physiological counterparts, new findings can readily be incorporated and tested for their influence on behavior. Interaction between biological and simulation experiments has been essential when developing this model and will continue to be so to extend its applicability.

Acknowledgements. I am grateful to Profs. Anders Lansner and Sten Grillner for supporting this work and for their valuable comments and suggestions on the manuscript. I would also like to thank Dr. Taifun Alishenas for his comments on the numerical methods and to Dr. Dean Pentcheff for kindly providing me with a number of useful references on fish hydrodynamics. This work was supported by the Swedish National Board for Industrial and Technical Development (NUTEK) project no. 89-01826P.

Appendix A: Derivation of the muscular torques

This appendix explains how the expression for the muscular torques (7) follows from the assumptions made in the text. Firstly, we assume that the length of the muscle fibers (L_L and L_R) varies linearly with the curvature of the body, for joint i represented by $(\varphi_{i+1} - \varphi_i)$:

$$L_L = k_1 + (\varphi_{i+1} - \varphi_i)k_2$$

$$L_R = k_1 - (\varphi_{i+1} - \varphi_i)k_2$$

(k_1, k_2, \dots denote arbitrary constants). Secondly, we assume that the muscles act as linear springs and dampers. Thus, the resulting forces from the left and right side muscles can be written:

$$\mu_L = L_L \xi_L + \dot{L}_L k_3 + k_4$$

$$\mu_R = L_R \xi_R + \dot{L}_R k_3 + k_4$$

where the dot means time derivative. Thirdly, we have assumed that the spring constants of the muscles (ξ_L and ξ_R) are linearly dependent on the activation of the corresponding motoneurons (M_L and M_R):

$$\xi_L = M_L k_5 + k_6$$

$$\xi_R = M_R k_5 + k_6$$

Since the muscle length varies linearly with the angle difference, it follows that the resulting torque also varies linearly with the forces. Therefore, the resulting torque from the two counteracting muscles can be expressed as:

$$T = (\mu_L - \mu_R)k_7$$

By inserting the expressions for μ_L , μ_R , L_L , and L_R , we get:

$$\begin{aligned} T = & ((k_1 + (\varphi_{i+1} - \varphi_i)k_2)(M_L k_5 + k_6) \\ & + (k_1 + (\varphi_{i+1} - \varphi_i)k_2)k_3 + k_4 \\ & - (k_1 - (\varphi_{i+1} - \varphi_i)k_2)(M_R k_5 + k_6) \\ & - (k_1 - (\varphi_{i+1} - \varphi_i)k_2)k_3 - k_4)k_7 \end{aligned}$$

which can be rewritten as:

$$\begin{aligned} T = & k_1 k_5 k_7 (M_L - M_R) \\ & + k_2 k_5 k_7 \left(M_L + M_R + \frac{2k_6}{k_5} \right) (\varphi_{i+1} - \varphi_i) \\ & + k_2 k_3 k_7 (\dot{\varphi}_{i+1} - \dot{\varphi}_i) \end{aligned}$$

By renaming the constant expressions $k_1 k_5 k_7 \rightarrow \alpha$, $k_2 k_5 k_7 \rightarrow \beta$, $2k_6/k_5 \rightarrow \gamma$, and $k_2 k_3 k_7 \rightarrow \delta$, we arrive at the final expression:

$$T = \alpha(M_L - M_R) + \beta(M_L + M_R + \gamma)(\varphi_{i+1} - \varphi_i) + \delta(\dot{\varphi}_{i+1} - \dot{\varphi}_i)$$

Appendix B: Matrix representation

This appendix defines the matrices and vectors used in the main text to describe the mechanical system and compute the inner forces.

The position and shape of the entire body is described by a $3N$ column vector $\bar{\mathbf{p}}$, and the speed of motion is given by a corresponding speed vector $\bar{\mathbf{v}}$:

$$\bar{\mathbf{p}} = [x_1, y_1, \varphi_1, x_2, y_2, \varphi_2, \dots, x_N, y_N, \varphi_N]^T$$

$$\bar{\mathbf{v}} = \dot{\bar{\mathbf{p}}} = [\dot{x}_1, \dot{y}_1, \dot{\varphi}_1, \dot{x}_2, \dot{y}_2, \dot{\varphi}_2, \dots, \dot{x}_N, \dot{y}_N, \dot{\varphi}_N]^T$$

The water forces and the muscle torques are combined in another $3N$ column vector $\bar{\mathbf{w}}$, and the inner forces are collected in a $2(N - 1)$ column vector $\bar{\mathbf{f}}$:

$$\bar{\mathbf{w}} = [W_{1,x}, W_{1,y}, T_1, W_{2,x}, W_{2,y}, T_2 - T_1, \dots,$$

$$W_{N,x}, W_{N,y}, -T_{N-1}]^T$$

$$\bar{\mathbf{f}} = [F_{1,x}, F_{1,y}, F_{2,x}, F_{2,y}, \dots, F_{N-1,x}, F_{N-1,y}]^T$$

The constraint equations (3) can be written in vector form as: $\bar{\mathbf{g}}(\bar{\mathbf{p}}) = \bar{\mathbf{0}}$, where $\bar{\mathbf{g}}(\bar{\mathbf{p}})$ is the following $2(N - 1)$ column vector:

$$\bar{\mathbf{g}}(\bar{\mathbf{p}}) = \begin{bmatrix} x_1 + \frac{l_1}{2} \cos \varphi_1 - x_2 + \frac{l_2}{2} \cos \varphi_2 \\ y_1 + \frac{l_1}{2} \sin \varphi_1 - y_2 + \frac{l_2}{2} \sin \varphi_2 \\ x_2 + \frac{l_2}{2} \cos \varphi_2 - x_3 + \frac{l_3}{2} \cos \varphi_3 \\ y_2 + \frac{l_2}{2} \sin \varphi_2 - y_3 + \frac{l_3}{2} \sin \varphi_3 \\ \vdots \end{bmatrix}$$

$\mathcal{G}(\bar{\mathbf{p}})$, a $3N \times 2(N - 1)$ matrix, is the transpose of the jacobian of $\bar{\mathbf{g}}(\bar{\mathbf{p}})$:

$$\mathcal{G}(\bar{\mathbf{p}}) \stackrel{\text{def}}{=} \left(\frac{\partial \bar{\mathbf{g}}(\bar{\mathbf{p}})}{\partial \bar{\mathbf{p}}} \right)^T$$

$$\mathcal{G}(\bar{\mathbf{p}}) = \begin{bmatrix} 1 & 0 & 0 & 0 & \dots \\ 0 & 1 & 0 & 0 & \dots \\ -\frac{l_1}{2} \sin \varphi_1 & \frac{l_1}{2} \cos \varphi_1 & 0 & 0 & \dots \\ -1 & 0 & 1 & 0 & \dots \\ 0 & -1 & 0 & 1 & \dots \\ -\frac{l_2}{2} \sin \varphi_2 & \frac{l_2}{2} \cos \varphi_2 & -\frac{l_2}{2} \sin \varphi_2 & \frac{l_2}{2} \cos \varphi_2 & \dots \\ 0 & 0 & -1 & 0 & \dots \\ 0 & 0 & 0 & -1 & \dots \\ 0 & 0 & -\frac{l_3}{2} \sin \varphi_3 & \frac{l_3}{2} \cos \varphi_3 & \dots \\ \vdots & \vdots & \vdots & \vdots & \ddots \end{bmatrix}$$

The mass matrix (a $3N \times 3N$ matrix) is simply:

$$\mathcal{M} = \begin{bmatrix} m_1 & 0 & 0 & 0 & 0 & 0 & \dots \\ 0 & m_1 & 0 & 0 & 0 & 0 & \dots \\ 0 & 0 & I_1 & 0 & 0 & 0 & \dots \\ 0 & 0 & 0 & m_2 & 0 & 0 & \dots \\ 0 & 0 & 0 & 0 & m_2 & 0 & \dots \\ 0 & 0 & 0 & 0 & 0 & I_2 & \dots \\ \vdots & \vdots & \vdots & \vdots & \vdots & \vdots & \ddots \end{bmatrix}$$

The second derivative (with respect to time) of the mechanical constraint equation (9) is:

$$\begin{bmatrix} \ddot{x}_1 - \ddot{\varphi}_1 \frac{l_1}{2} \sin \varphi_1 - \dot{\varphi}_1^2 \frac{l_1}{2} \cos \varphi_1 - \ddot{x}_2 - \ddot{\varphi}_2 \frac{l_2}{2} \sin \varphi_2 - \dot{\varphi}_2^2 \frac{l_2}{2} \cos \varphi_2 \\ \ddot{y}_1 + \ddot{\varphi}_1 \frac{l_1}{2} \cos \varphi_1 - \dot{\varphi}_1^2 \frac{l_1}{2} \sin \varphi_1 - \ddot{y}_2 + \ddot{\varphi}_2 \frac{l_2}{2} \cos \varphi_2 - \dot{\varphi}_2^2 \frac{l_2}{2} \sin \varphi_2 \\ \ddot{x}_2 - \ddot{\varphi}_2 \frac{l_2}{2} \sin \varphi_2 - \dot{\varphi}_2^2 \frac{l_2}{2} \cos \varphi_2 - \ddot{x}_3 - \ddot{\varphi}_3 \frac{l_3}{2} \sin \varphi_3 - \dot{\varphi}_3^2 \frac{l_3}{2} \cos \varphi_3 \\ \ddot{y}_2 + \ddot{\varphi}_2 \frac{l_2}{2} \cos \varphi_2 - \dot{\varphi}_2^2 \frac{l_2}{2} \sin \varphi_2 - \ddot{y}_3 + \ddot{\varphi}_3 \frac{l_3}{2} \cos \varphi_3 - \dot{\varphi}_3^2 \frac{l_3}{2} \sin \varphi_3 \\ \vdots \end{bmatrix} = \bar{\mathbf{0}}$$

This can be rewritten as:

$$\begin{bmatrix} 1 & 0 & -\frac{l_1}{2} \sin \varphi_1 & -1 & 0 & -\frac{l_2}{2} \sin \varphi_2 & \dots \\ 0 & 1 & \frac{l_1}{2} \cos \varphi_1 & 0 & -1 & \frac{l_2}{2} \cos \varphi_2 & \dots \\ 0 & 0 & 0 & 1 & 0 & -\frac{l_2}{2} \sin \varphi_2 & \dots \\ 0 & 0 & 0 & 0 & 1 & \frac{l_2}{2} \cos \varphi_2 & \dots \\ \vdots & \vdots & \vdots & \vdots & \vdots & \vdots & \ddots \end{bmatrix} \cdot \begin{bmatrix} \ddot{x}_1 \\ \ddot{y}_1 \\ \ddot{\varphi}_1 \\ \ddot{x}_2 \\ \ddot{y}_2 \\ \ddot{\varphi}_2 \\ \vdots \end{bmatrix} = \begin{bmatrix} \dot{\varphi}_1^2 \frac{l_1}{2} \cos \varphi_1 + \dot{\varphi}_2^2 \frac{l_2}{2} \cos \varphi_2 \\ \dot{\varphi}_1^2 \frac{l_1}{2} \sin \varphi_1 + \dot{\varphi}_2^2 \frac{l_2}{2} \sin \varphi_2 \\ \dot{\varphi}_2^2 \frac{l_2}{2} \cos \varphi_2 + \dot{\varphi}_3^2 \frac{l_3}{2} \cos \varphi_3 \\ \dot{\varphi}_2^2 \frac{l_2}{2} \sin \varphi_2 + \dot{\varphi}_3^2 \frac{l_3}{2} \sin \varphi_3 \\ \vdots \end{bmatrix}$$

which can be identified as $\mathcal{G}^T \ddot{\mathbf{v}} = \ddot{\pi}$ with π defined as the right hand side above.

References

Alishenas T (1992) Zur numerischen Behandlung, Stabilisierung durch Projektion und Modellierung mechanischer Systeme mit Nebenbedingungen und Invarianten. PhD thesis, Royal Institute of Technology, Stockholm, 1992

Blake RW (1983) Fish locomotion. Cambridge University Press, London

Blevins RD (1984) Applied fluid dynamics handbook. Van Nostrand Reinhold, New York

Bowtell G, Williams T (1991) Anguilliform body dynamics: modelling the interaction between muscle activation and body curvature. *Phil Trans R Soc Lond B* 334:385–390

Brodin L, Grillner S, Rovainen CM (1985) *N*-methyl-D-spartate (NMDA), kainate and quisqualate receptors and the generation of fictive locomotion in the lamprey spinal cord. *Brain Res* 325:302–306

Brodin L, Tråvén H, Lansner A, Wallén P, Ekeberg Ö, Grillner S (1991) Computer simulations of *N*-methyl-D-aspartate (NMDA) receptor induced membrane properties in a neuron model. *J Neurophysiol* 66:473–484

Buchanan JT (1992) Neural network simulations of coupled locomotor oscillators in the lamprey spinal cord. *Biol Cybern* 66:367–374

Ekeberg Ö, Stensmo M, Lansner A (1990) SWIM – a simulator for real neural networks. Technical report TRITA-NA-P9014, Dept. of Numerical Analysis and Computing Science, Royal Institute of Technology, Stockholm, Sweden

Ekeberg Ö, Wallén P, Lansner A, Tråvén H, Brodin L, Grillner S (1991) A computer based model for realistic simulations of neural networks. I. The single neuron and synaptic interaction. *Biol Cybern* 65:81–90

Gray DE (ed) (1972) American Institute of Physics handbook, 3rd edn. McGraw-Hill, New York

Gray J (1933a) Directional control of fish movement. *Proc Roy Soc B* 113:115–125

Gray J (1933b) Studies in animal locomotion. I. The movement of fish with special reference to the eel. *J Exp Biol* 10:88–103

Gray J (1968) Animal locomotion. Weidenfeld and Nicolson, London

Grillner S (1974) On the generation of locomotion in the spinal dogfish. *Exp Brain Res* 20:459–470

Grillner S (1981) Control of locomotion in bipeds, tetrapods and fish. In: Brooks VB (ed), *Handbook of physiology*, sect 1, vol 2. American Physiological Society, Bethesda, Md, pp 1179–1236

Grillner S, Kashin S (1976) On the generation and performance of swimming in fish. In: Herman RM, Grillner S, Stein PSG, Stuart DG (eds) *Neural control of locomotion*. Plenum, New York, pp 181–201

Grillner S, McClellan AD, Perret C (1981a) Entrainment of the spinal pattern generators for swimming by mechanosensitive elements in the lamprey spinal cord in vitro. *Brain Res* 217:380–386

Grillner S, McClellan AD, Sigvardt K, Wallén P, Wilén M (1981b) Activation of NMDA receptors elicits “fictive locomotion” in lamprey spinal cord in vitro. *Acta Physiol Scand* 113:549–551

Grillner S, McClellan A, Sigvardt K (1982) Mechanosensitive neurons in the spinal cord of the lamprey. *Brain Res* 235:169–173

Grillner S, Wallén P, Brodin L, Lansner A (1991) Neuronal network generating locomotor behavior in lamprey: circuitry, transmitters, membrane properties and simulations. *Ann Rev Neurosci* 4:169–199

Kalveram KT (1991) Controlling the dynamics of a two-jointed arm by central patterning and reflex-like processing. *Biol Cybern* 65:65–71

Lacquaniti F, Soechting JF (1986) Simulation studies on the control of posture and movement in a multi-jointed limb. *Biol Cybern* 54:367–378

Lighthill J (1969) Hydromechanics of aquatic animal propulsion. *Ann Rev Fluid Mech* 1:413–445

Matsushima T, Grillner S (1992) Neural mechanisms of intersegmental coordination in lamprey: local excitability changes modify the phase coupling along the spinal cord. *J Neurophysiol* 67:373–388

Ólafsson Ö, Alishenas T (1992) A comparative study of the numerical integration and velocity stabilization of two mechanical test problems. Technical report TRITA-NA-9210, Dept of Numerical Analysis and Computing Science, Royal Institute of Technology, Stockholm, Sweden

Taga G, Yamaguchi Y, Shimizu H (1991) Self-organized control of bipedal locomotion by neural oscillators in unpredictable environment. *Biol Cybern* 65:147–159

Tax AAM, Denier van der Gon JJ (1991) A model for neural control of gradation of muscle force. *Biol Cybern* 65:227–234

Taylor G (1952) Analysis of the swimming of long and narrow animals. *Proc Roy Soc Lond A* 214:158–183

Viana Di Prisco G, Wallén P, Grillner S (1990) Synaptic effects of intraspinal stretch receptor neurons mediating movement-related feedback during locomotion. *Brain Res* 530:161–166

Wadden T, Grillner S, Matsushima T, Lansner A (1993) Undulatory locomotion – simulations with realistic segmental oscillator. In: Eeckman FM, Bower JM (eds), *Computations & neural systems* 92. Kluwer, Boston

Wallén P, Williams T (1984) Fictive locomotion in the lamprey spinal cord in vitro compared with swimming in the intact and spinal animal. *J Physiol (Lond)* 347:225–239

Wallén P, Ekeberg Ö, Lansner A, Brodin L, Tråvén H, Grillner S (1992) A computer-based model for realistic simulations of neural networks. II. Simulation of the segmental network generating locomotor rhythmicity in the lamprey. *J. Neurophysiol* 68:1939–1950

Webb PW, Weihls D (1983) Fish biomechanics. Praeger, New York

Williams TL (1992) Phase coupling by synaptic spread in chains of coupled neuronal oscillators. *Science* 258:662–665

Williams TL, Grillner S, Smoljaninov VV, Wallén P, Kashin S, Rossignol S (1989) Locomotion in lamprey and trout: the relative timing of activation and movement. *J Exp Biol* 143:559–566

Wu TY-T (1971) Hydromechanics of swimming propulsion. *J Fluid Mech* 46:337–355, 521–568

Yates GT (1983) Hydrodynamics of body and caudal fin propulsion. In: Webb PW, Weihls D (eds) *Fish biomechanics*. Praeger, New York, pp 177–213